Slow and fast crystallising poly aryl ether ketones (PAEKs) in 3D printing: crystallisation kinetics, morphology, and mechanical properties

Nan Yi, Richard Davies, Adam Chaplin, Paul McCutchion, Oana Ghita

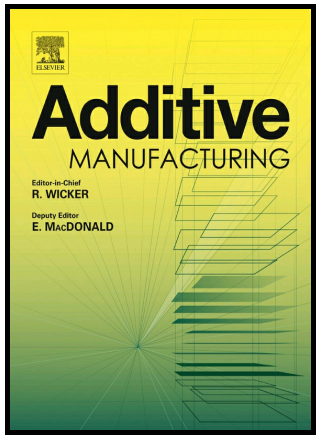

PII: S2214-8604(21)00008-7

DOI: https://doi.org/10.1016/j.addma.2021.101843

Reference: ADDMA101843

To appear in: *Additive Manufacturing*

Received date: 24 June 2020
Revised date: 18 December 2020
Accepted date: 5 January 2021

Please cite this article as: Nan Yi, Richard Davies, Adam Chaplin, Paul McCutchion and Oana Ghita, Slow and fast crystallising poly aryl ether ketones (PAEKs) in 3D printing: crystallisation kinetics, morphology, and mechanical properties, *Additive Manufacturing,* (2020) doi:https://doi.org/10.1016/j.addma.2021.101843

Slow and fast crystallising poly aryl ether ketones (PAEKs) in 3D printing: crystallisation kinetics, morphology, and mechanical properties

Nan Yi[1*], Richard Davies[1], Adam Chaplin[2], Paul McCutchion[1], Oana Ghita[1]

1 College of Engineering, Mathematics and Physical Sciences, University of Exeter, Exeter, EX4 4QF, UK

2 Victrex PLC, Hillhouse international, Thornton Cleveleys, Lancashire, FY5 4QD, UK

* E-mail: N.Yi@exeter.ac.uk

Abstract

Poly aryl ether ketone (PAEK) polymers are gaining interest in 3D printing for their good mechanical properties and high service temperatures. The aim of this study was to compare the crystallisation kinetics, morphology, and mechanical properties of two different PAEK polymers used in fused filament fabrication (FFF), i.e. the fast crystallising PEEK151 (poly ether ether ketone) grade originally designed for injection moulding and the slow crystallising AM 200 grade tailored specifically for FFF. The crystallisation kinetics of both grades were examined across a wide temperature range. A method to select annealing temperatures and annealing times based on the intrinsic crystallisation behaviour of each polymer was proposed. The dual-Avrami model highlighted a different crystallite growth for AM 200 in comparison with PEEK151 with a higher rate of secondary crystallisation. Lamellar thicknesses were measured by SAXS and calculated via the Thomson-Gibbs equation. The lamellar thicknesses of primary and secondary crystallisation for AM 200 showed a stronger temperature dependence with steeper slopes when increasing the isothermal temperature. The benefit of using a slow crystallising PAEK polymer over the conventional fast crystallising grades is evidenced by the improvement of Z strength which enhances the overall isotropy of printed parts.

1. Introduction

Owing to their superior mechanical properties and thermal stability, poly aryl ether ketone (PAEK) polymers are widely used as high performance engineering thermoplastics [1][2]. During the last three decades, a large number of additive manufacturing (AM) technologies have been developed for thermoplastic materials and within this large family some of the

systems are suitable for fabrication of PAEK parts [3][4][5]. Fused filament fabrication (FFF) systems typically require smaller set up and running costs than powder bed systems, and the expiration of key patents enabling commercial opportunities for multiple new businesses has been critical to FFF becoming a fast-growing polymer AM technology. By extruding solid filament through a computer-controlled hot nozzle onto a building plate, the system creates parts layer by layer. For many engineering applications, 100% dense parts are desired, a property very difficult to achieve with many FFF systems. Porosity is considered inevitable due to the deposition through a circular nozzle. By altering flow rate, raster gap, and building orientation, Rodriguez et al [6] printed ABS parts with porosity ranging from 2% to 16% using a Stratasys FDM1600 Modeller. Later Too et al [7] and Ang et al [8] deliberately applied this technique in tissue engineering to create porous ABS scaffolds with porosity between 7.6% to 82.9%. Using an Ultimaker 3 system, Liao et al [9] was able to print PLA bars with low porosity (~1.5%) throughout the top layers whilst high porosity (~25%) through the middle and bottom layers. Most recently, Bond High Performance 3D Technology is developing a void-free FFF system [10]. This advanced system has the potential to improve the mechanical properties of FFF products to a new level.

Another sought after property of these systems and materials is Z strength values similar to those in the X-Y directions. Arif et al [11] and Rinaldi et al [12] reported that the Z strength values are usually 13% - 25% of X-Y strength values when following the same printing strategy. Because Z strength value is directly linked to the layer to layer bonding and the rate of crystallisation at the layer interface, several studies have tried to model the layer to layer bonding and understand the effect of thermal processing conditions [13][14].

Many of the current FFF systems are design to use existing commercial PEEK grades such as Victrex PEEK 450G [11][12][13][15] and Victrex PEEK 150 [14]. These PEEK materials are optimised and tailored in terms of molecular weight, viscosities and crystallisation kinetics for injection moulding or bulk extrusion processes rather than filament-based layer by layer deposition process. The crystallisation kinetics of PEEK 450 has been extensively studied, although in many cases it was done in isolation, without linking its crystallisation behaviour to the actual manufacturing processes, including heating and cooling rates involved in specific processes [16][17][18][19]. In some other studies, efforts have been made to investigate the relationship between crystallisation and manufacturing process. Lustiger et

al [20] demonstrated how to select compression moulding and ageing conditions for PEEK plaques based on crystallisation behaviours. In addition, Berretta et al [21] proposed a method to predict the laser sintering processing window from the inherent thermal behaviours of PEEK powders. The majority of existing literature is focused on developing systems and adjusting processing plus post-processing conditions to make existing polymeric grades perform and achieve desirable crystallinity levels and morphologies [22][23][24][25][26][27], rather than adjusting the polymer to better suit the system requirements (e.g. processing parameters).

Regarding the FFF process, amorphous polymers have made somewhat more progress, and in many cases seem to provide relatively isotropic properties as 3D printed parts in comparison with the semi-crystalline polymers. For example, Polyetherimide (PEI) known as Ultem 9085 has been applied in high temperature FFF processes. The work of Bagsik et al [28] showed that the Z strength value of Ultem 9085 tensile bars could reach approximately 60% of its X strength value. Similar results were also reported by Fischer and Schoppner [29]. In addition, the shrinkage created by the crystallisation process is removed in amorphous structures, allowing better exploration of design freedom offered by the technology. Learning from pure amorphous polymers, slow crystallising semi-crystalline polymers had recently been developed for use with FFF systems. PEKK grades (such as ThermaX® PEKK-C filaments [30]) can be printed amorphously followed by annealing to initiate and to accelerate the crystallisation process, layer to layer bonding, and the overall strength of the parts. Although the improvement on bonding strength has been confirmed for amorphous PEEK films via lap-shear tests [31], there is no literature investigating the effect of slow crystallising polymers on layer to layer bonding.

Annealing is a well-established method to improve the mechanical performance of conventional moulded PAEK products. Talbott et al [32] concluded that the annealing process increased tensile and compressive strength in comparison with non-treated specimens of the same crystallinity level. However, no visible improvement was found regarding moduli, the fracture toughness, or shear properties. Cebe [33] observed that annealing leads to increased long period and greater crystal perfection. Jar et al [34] adopted this theory to explain the increase of yield stress. Moreover, annealing results in

slower creep and stress relaxation, mainly associated with the restricted molecular mobility [27][34].

But so far, very little is known on the annealing effects on polymer 3D printed parts. In injection moulding, the parts are 100% dense with little anisotropy whilst the majority of the FFF processes create controlled or un-controlled porosity and highly anisotropic parts. When exposed to heat and allowed to crystallise, the shrinkage created by the crystallisation process as well as the material thermal shrinkage can distort parts. A recent paper of Kurtz et al [35] attempts to consider annealing as a method of improving mechanical strength of 3D printed parts but the crystallisation kinetics are not discussed. The results show no significant difference of porosity. At slow printing speed, annealing has a negative effect on the ultimate load/torque, whilst no effect at all at high printing speed. These results are not surprising considering the fast crystallisation rate of PEEK 450, which is the material chosen by the authors for investigation. So far, the annealing protocols for such polymers in combination with the FFF processes have not been thoroughly investigated and understood. This study is investigating, by comparison, the crystallisation kinetics of two PAEK polymers in the context of an FFF process: Victrex PEEK 151 – an injection moulding grade and Victrex AM 200 – an FFF tailored grade. The paper is also discussing the method of selection of annealing temperature and time, based on the inherent crystallisation kinetics. The effects of crystallisation mechanisms and annealing on mechanical properties are also reported. Combined with morphological examinations, a detailed insight can be gained, to help design dedicated polymers for the FFF process.

2. Materials and experimental

2.1 Materials

Two materials have been used for this study: 1) Victrex PEEK 151 and 2) Victrex AM 200. The material properties are displayed in Table 1. Victrex PEEK 151 filaments were purchased from 3D4Makers. Victrex AM 200 filaments were provided by Victrex.

PEEK151 is synthesized through conventional nucleophilic aromatic substitution reaction with 100% aromatic dihalides monomer. AM 200 is a fully aromatic PEEK based poly aryl ether ketone copolymer. The molecular structure of AM 200 has been designed to improve the rheological and crystallisation characteristics for use in FFF. As shown in Figure 1, the

molecular backbone of AM 200 has a higher concentration of aryl groups than PEEK151, causing a reduced chain mobility. This chemical structure has led to a polymer with a lower melting temperature (T_m) and slower crystallisation rate but higher glass transition temperature (T_g) as shown in Table 1.

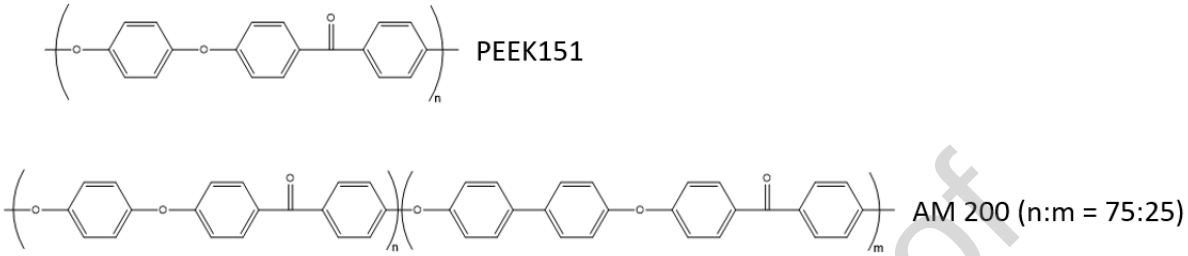

Figure 1. Chemical structures of PEEK151 and AM 200.

Table 1. Material properties of Victrex PEEK 151 and Victrex AM 200.

Material	**T_m(°C)**	**T_g(°C)**	**Shear Viscosity (Pa.s)***	**Filament Diameter (mm)**
Victrex PEEK 151	346	140	130	1.75
Victrex AM 200	304	156	250	1.75

* At 400°C and a shear rate of 1000 s^{-1}

2.2 Sample preparations

2.2.1 FFF printing

Dog-bone shaped tensile bars were printed using a 3DGence INDUSTRY F340 according to ISO 527-2 Type 1A. Crystalline filaments were employed for their high stiffness and low friction to avoid blockage during printing. Three build orientations, i.e. flat, side, and vertical (Z), were made as illustrated in Figure 2. All bars were printed on top of a 3-layer dissolvable raft through a HTmax module with nozzle diameter of 0.4 mm. The infill was set as 100% and layer thickness of 0.15 mm. The printing speed was 30 mm/s. Toolpaths were generated by 3DGence Slicer 1.3.2. Temperature settings for each material are summarised in Table 2. In later experiments, all samples were tested as printed. No other post-processing except annealing was applied to the fabricated samples.

During printing, the bed temperature (100 °C) and chamber temperature (60 °C) were below the Tg (>140 °C) of PAEKs. As molecular chain mobility is restricted at this level, the

annealing brought by bed temperature or chamber temperature has no effect on the mechanical properties. As supported by the work of Arzak et al [25], annealing PEEK at 100 °C even for 24 hours has nearly no impact on its modulus, strength, or elongation at break. Therefore, in our study, build orientation is the major factor causing mechanical anisotropy rather than thermal history. This conclusion justifies the discussion on improvement on isotropy in Section 3.3.

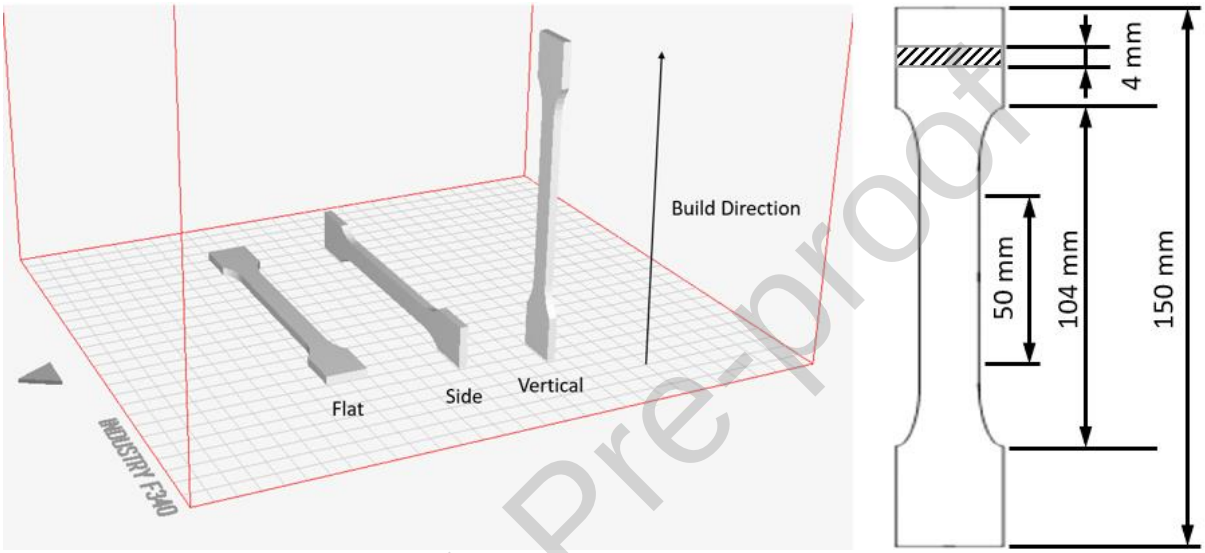

Figure 2. Build orientation and dimensions of tensile specimens.

Table 2. Processing and post-processing parameters.

Material	Printing				Annealing		
	Bed (°C)	Nozzle (°C)	Chamber (°C)	Build orientation	Temperature (°C)		Time (hr)
					LAT*	HAT*	
Victrex PEEK151	100	410	60	Flat, Side, Vertical	156	200	2, 4
Victrex AM 200	100	380	60	Flat, Side, Vertical	170	200	2, 4

* LAT – low annealing temperature; HAT – high annealing temperature.

2.2.2 Annealing

The annealing temperatures are classified into two groups. The first group is the LAT (low annealing temperature), i.e. 156 °C for PEEK151 and 170 °C for AM 200. These two annealing temperatures were selected based on the thermal analysis in Section 3.1, so that PEEK151 and AM 200 would have similar crystallisation speeds (both with half-times around 650 s). The LATs are among the lowest annealing temperatures that can be chosen to allow crystallisation to be finished within 2 hours. They were selected to ensure a slow but

complete crystallisation within two hours, minimising warping caused by rapid heating/crystallisation. The second group is the HAT (high annealing temperature), i.e. 200 °C for both PAEK grades, which is commonly selected in other studies [27][35].

During annealing, all the samples were buried in a sandbox to ensure uniform thermal conditions. A thermocouple was inserted into the quartz sand to accurately monitor the annealing temperature and precisely control the annealing time. At the end of the desired annealing time, samples were quenched in water to stop the annealing process.

2.3 Thermal analysis - crystallisation kinetics based on DSC and Flash DSC

2.3.1 Conventional DSC

The differential scanning calorimetry (DSC) measurements were performed using a METTLER TOLEDO differential scanning calorimeter. Printed parts and filaments were examined. For each scan, approximately 10 mg mass of material was weighed and encapsulated in a standard Aluminium pan, crimping with a standard Aluminium lid. All tests were purged using a Nitrogen flow at 50 ml/min.

Melting and cooling behaviours were studied via a standard dynamic scanning sequence including one heating ramp from 25 °C to 450 °C and one cooling ramp from 450 °C to 25 °C. The heating/cooling rate was 10 °C/min during scanning.

To investigate the crystallisation kinetics, a cold-crystallisation isothermal test protocol for the lower temperature region and an isothermal from melt test protocol for the high temperature region were designed. At the low temperature region, the sample was heated from 25 °C to the selected isothermal temperature at 60 °C/min. At the high temperature region, the sample was first heated to 400 °C for 1 min to remove the thermal history, then cooled to the desired isothermal temperature at 60 °C/min.

2.3.2 Flash DSC

A METTLER TOLEDO Flash DSC 2+ with UFS 1-type chip sensors were used for investigating crystallisation kinetics in the fast crystallisation region. Before preparing samples, all chip sensors went through conditioning and thermocouple correction. A 20 µm thick slice was first sectioned from the tip of a filament using a razor blade microtome, then it was cut into a square with length less than 100 µm by a scalpel. This tiny film was placed onto the chip

sensor using a brush pen hair. A pre-melt heating cycle at 0.5 °C/s to 310 °C was used to mount the sample firmly on the centre of the chip and to ensure good thermal contact. During testing, the atmosphere was protected by a Nitrogen flow at 80 ml/min.

In this fast crystallisation temperature region, two test protocols were designed. A direct isothermal test protocol was employed when the exothermic crystallisation peak during the isothermal stage is large enough to be detected. From experimental observation this protocol applied to crystallisations finished within 20 seconds. Crystallisation process lasting longer than 20 seconds generated a flat exothermic peak that was hardly detectable by the instrument. In this case, a discontinuous isothermal test protocol was applied.

In the direct isothermal test protocol, the sample was heated up to a melting temperature (400°C for Victrex PEEK151 and 370°C for Victrex AM 200) for 1 s to remove the thermal history then cooled to the isothermal temperature. The isothermal stage was held for 20 seconds before quenching to 30 °C. Both heating rate and cooling rate were 1000 °C/s. In the discontinuous isothermal test protocol, the same ramping cycle as in the direct protocol was repeated with various isothermal times. Until a stable value of enthalpy was reached, endothermic melting peaks extracted from each following heating segment were used to estimate the degree of cumulative crystallinity.

To summarise, the proper instruments and thermal test protocols linked to temperature regions are listed in Table 3.

Table 3. Thermal methods for temperature regions.

Material	**Conventional DSC**		**Flash DSC**
	cold-crystallisation isothermal test protocol	**isothermal from melt test protocol**	
PEEK 151	150 – 165 °C	300 – 330 °C	170 – 300 °C
AM 200	160 – 180 °C	260 – 290 °C	180 – 260 °C

2.4 SAXS

The small angle X-ray scattering measurements were performed on a laboratory beamline device SAXSpoint 2.0 (Anton Paar, Austria) equipped with a CuKα radiation source (wavelength 1.541 Å) and a 2D area detector. As printed and annealed specimens were mounted using a Solid Sampler (Anton Paar, Austria) on a VarioStage (Anton Paar, Austria).

The scattering intensity was captured in one frame of 30 minutes exposure time. All measurements were performed under vacuum.

SAXSanalysis software (Anton Paar, Austria) was used to analyse the data. Corrections on scattering intensities were made regarding the transmission mode and the background scattering. Two-dimensional data was converted to one-dimensional data after the corrections.

2.5 Mechanical tests

Uniaxial tensile tests were performed to characterise the stress-strain behaviour. All tests were performed at room temperature. Moduli were measured under a constant speed at 1 mm/min, whilst tensile strengths and elongations at break were measured at 5 mm/min. All the specimens were tested by a 20 KN capacity standard tensile/compression machine (SHIMADZU®). From 3 to 10 repeats were carried out for each build orientation and each polymer. Statistical analysis was performed using JMP software (SAS, Version 15.0.0). One-way ANOVA for single factor analysis and Tukey-Kramer HSD for means comparisons was performed to identify any significant differences below the criteria of 0.05.

3. Results and Discussions

3.1 Crystallisation kinetics

The DSC thermograms in the upper half of Figure 3 show that the AM200 parts, printed amorphously, go through a cold crystallisation transition at approximately 190°C prior to melting. The temperature position of the peaks related with the cold crystallisation, melting and crystallisation from melt were used as a guide to define the isothermal crystallisation methods required to measure the crystallisation half-times displayed in the bottom half of Figure 3. The discussions on crystallisation half-times are detailed in the later part of this section, with respect to the results presented in Figure 4 and Figure 5.

Between 160°C and 300°C, three thermal regions separated by four characteristic temperatures were identified. Region I ($T_1 < T < T_2$): measuring isothermal crystallisation prior to cold crystallisation using a conventional DSC; Region II ($T_2 < T < T_3$): including crystallisation transitions which are normally fast and require the use of Flash DSC and Region III ($T_3 < T < T_4$): focused on isothermal crystallisation temperatures defined by the

onset of melting and onset of crystallisation from melt, analysis carried out using a conventional DSC. Details of each test protocol are included in Section 2.3. From thermal phase transitions, it is noted that T_1 is close to the glass transition temperature; T_2 corresponds to the onset of cold crystallisation; T_3 is near the crystallisation peak from melting and T_4 slightly surpasses the onset of melting.

As crystallisation time varies from seconds to hours, it is a common practice to adopt various instruments and test protocols to capture crystallisation behaviours in a wide temperature range. However, how to choose the proper method remains vague [36][37][38]. In Figure 3 we demonstrated that the temperature regions can be associated with certain characteristic temperatures of thermal phase transitions. This proposed approach has given a clear guidance on instrument/protocol selection and can be generally applied to other semi-crystalline polymers.

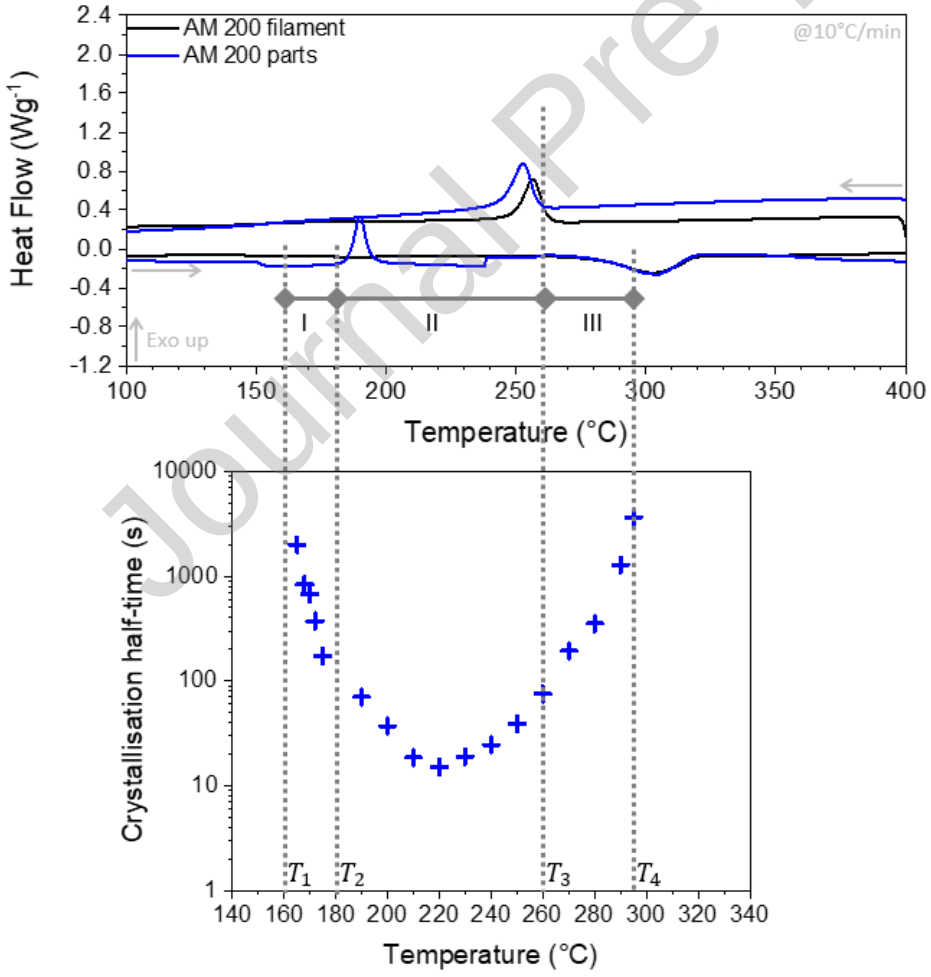

Figure 3. DSC thermograms of Victrex AM 200 before and after printing, correlating the temperature regions with the thermal phase transitions.

Figure 4 shows the crystallisation half-times, calculated from the exothermic heat flow integration in isothermal thermograms [39], across the entire temperature region (150 - 330°C) for the two polymers: PEEK151 and AM 200. An example of the isothermal thermogram and the detailed procedures to calculate crystallisation half-times can be found in the supplementary materials. The new grade AM 200 shows significantly slower crystallisation kinetics across the entire temperature region tested. At 220°C, the AM 200 PAEK grade takes approximately 10 times longer to reach crystallinity C(t) = 50% in comparison with the PEEK151 grade.

When applied to PAEKs, the conventional Avrami model of crystallisation tends to show discrepancies between the measured data and the model in the final stages of crystallisation (> 95%) [19][39]. It is due to the fact that PAEKs are highly sensitive to the equilibrium between crystalline and non-crystalline phases and it has been postulated that the final structure is the result of a two-stage process. Two of the most relevant models considering the two-stage crystallisation process are the dual-Avrami model introduced by Velisaris and Seferis in 1986 [40] and the Hillier model introduced in 1965 [41]. The dual-Avrami model assumes that the two stages of crystallisation co-exist as two simultaneous phases, each becoming dominant at different times within the crystallisation process. The Hillier model considers that the two processes are consecutive, the conventional Avrami crystallisation process occurs first followed by a first order crystallisation stage that grows from the primary crystallisation.

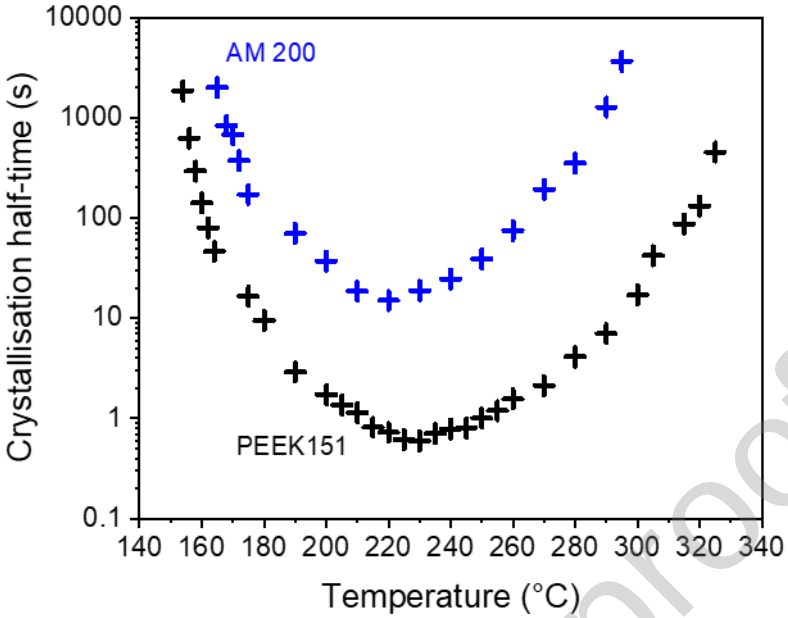

Figure 4. Crystallisation half-time of PEEK151 and AM 200 as a function of isothermal temperature.

In this study, a dual Avrami model was employed to investigate the crystallisation kinetics. The dual Avrami model is defined by Eq. 1 [40]:

$$C(t) = P_1[1 - exp(-K_1 t^{n_1})] + P_2[1 - exp(-K_2 t^{n_2})] \quad \text{(Eq. 1)}$$

where $C(t)$ is the relative crystallinity, K_1 and K_2 are the crystallisation rate constants, n_1 and n_2 are the Avrami exponents for the primary and secondary stage of crystallisation, respectively. P_1 and P_2 represent the probability of the primary and secondary stage of crystallisation.

Considering primary crystals grow in an amorphous phase whilst secondary crystallisation in a semi-crystalline structure, $P_1 = 1 - C(t)$ is proportional to the amorphous fraction and $P_2 = C(t)$ is proportional to the crystallinity fraction [38]. At the point where the dominance of primary crystallisation gives way to secondary crystallisation, both stages have the same probability $P_1 = P_2$ and hence $C(t) = 0.5$ at this point. Substituting the above relations back into Eq. 1 reduces the fitting parameters from five to three [38]. This approach increases the robustness of the Avrami exponents and the crystallisation rate constants obtained by fitting the dual-Avrami model with experimental data.

Experimental data of PEEK151 and AM 200 and dual-Avrami model fittings in Region I are presented in Figure 5 as examples. It shows that the dual-Avrami model is a good fit for the isothermal crystallisation measurements for both PAEK grades, where the secondary crystallisation behaviours are successfully captured.

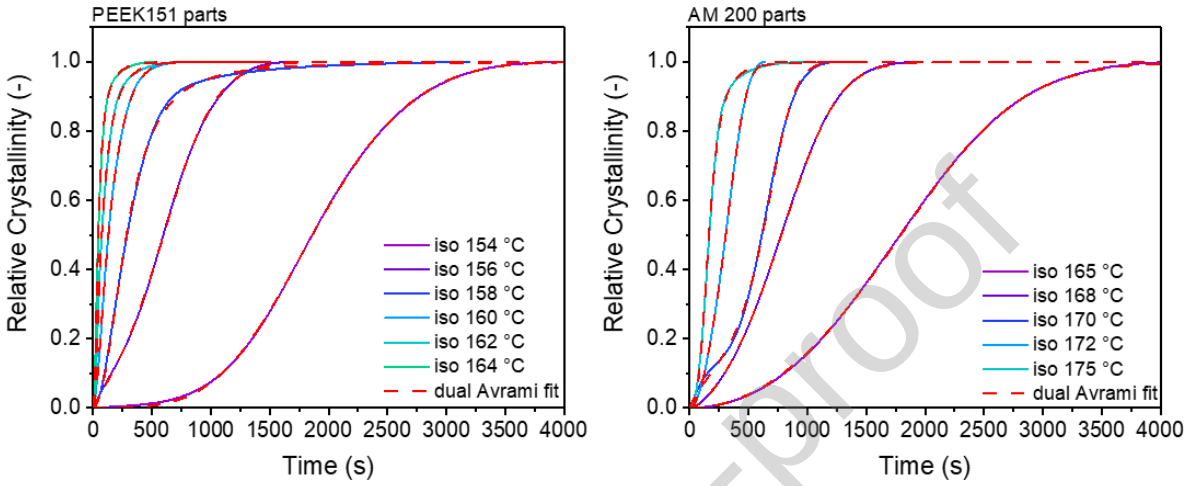

Figure 5. Experimental data and dual-Avrami model fittings of PEEK151 and AM 200 in Region I.

It has been attempted to separate the evolution of primary and secondary crystallisation for PAEK materials [19][42]. Their efforts support the idea that primary crystallisation dominates at the beginning and secondary crystallisation dominates at the end.

The Avrami kinetic coefficients (K_1 and K_2) were calculated for both PEEK151 and AM 200 and plotted as a function of isothermal temperature in Figure 6. PEEK151 shows similar rate constants for primary (K_1) and secondary (K_2) crystallisation. The bell-shape curves mirror the crystallisation half-time trace, highlighting that both stages of crystallisation have the highest rate between 200 and 260°C.

In the case of AM 200, the rate constants differ significantly: the rate constants for the primary stage of crystallisation (K_1) were not influenced by the isothermal temperatures, whereas the secondary crystal growth rates (K_2) were significantly higher in the same temperature range as was seen with PEEK151, from 200 to 260 °C.

The rate constants could be an indication that the primary crystallisation stage of AM 200 is less sensitive to isothermal temperature and has a different growth behaviour when

compared with PEEK151. The bell-shape curve of rate constants has been reported for PAEK materials [37][42].

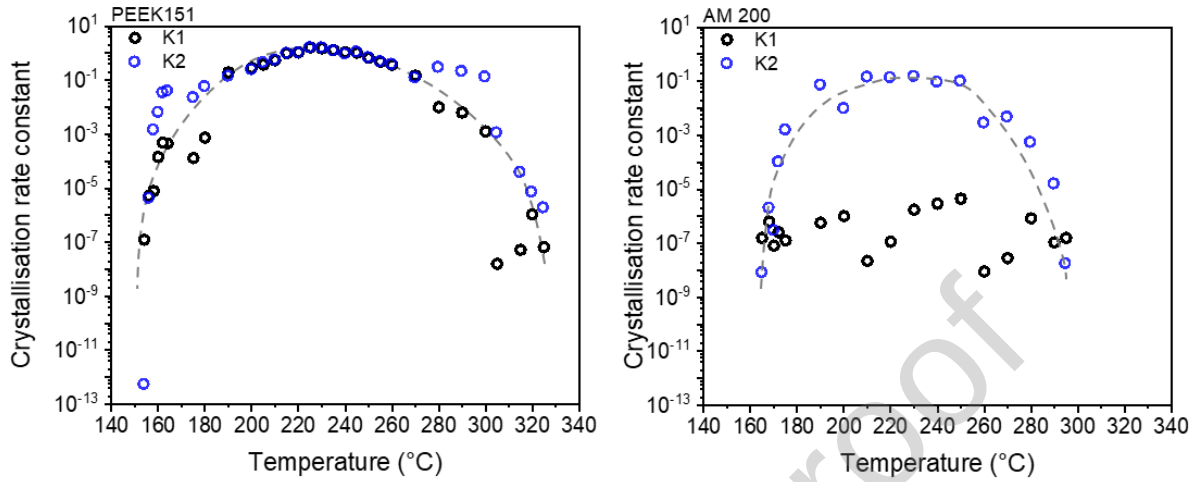

Figure 6. Avrami kinetic coefficient of PEEK151 and AM 200 as a function of isothermal temperature. Dash lines are guides to the eye.

The Avrami exponents for PEEK151 and AM 200 are presented in Figure 7. The primary Avrami exponent n_1 for AM 200 has a higher average value (3.7) when compared with the primary Avrami exponent for PEEK151 (2.4).

The faster crystallisation of PEEK151 evidenced by the crystallisation half-time and the constant rates, seems to indicate that the PEEK151 crystals are less developed, have a less defined spherulitic structure at the end of the nucleation process in comparison with AM 200, which has a slower nucleation during primary crystallisation and a better spherulitic structure.

The secondary crystallisation creates one-dimensional crystal structures for both materials as shown by the secondary Avrami exponents values n_2 as 1.2 for AM 200 and 1.6 for PEEK151.

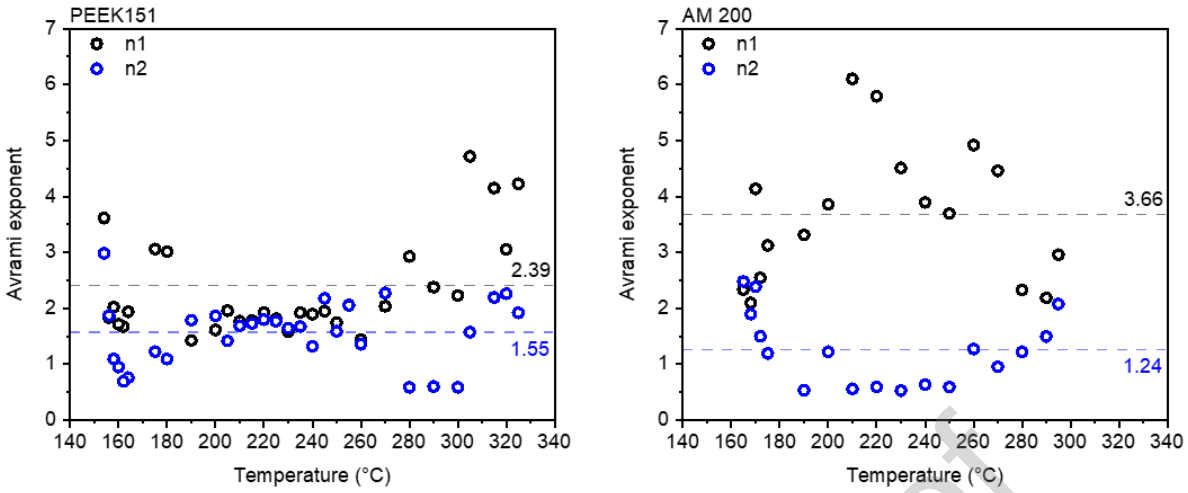

Figure 7. Avrami exponent of PEEK151 and AM 200 as a function of isothermal temperature. Dash lines represent the average.

The morphology of the crystals and its correlation with the Avrami exponents are well documented in literature [43], n values of 1 define one-dimensional crystal structures, values between 2 and 3 are related with disk like spherulites and between 3-4 with three-dimensional spherulites.

The dual-Avrami model has revealed that PEEK151 and AM 200 present significantly different crystallisation kinetics. The impact of these kinetics will be studied further regarding crystal morphology and mechanical properties in the following sections.

3.2 Crystalline morphology

Previous annealing research on PEEK has only a general guidance on how to select the annealing temperature: above the T_g and below the degradation temperature [26][27][34][35]. In this study, two annealing temperatures were selected for each PAEK grades, as explained in Section 2.2.2: LAT in Region I corresponding to a crystallisation half-time of 650 s (i.e. 156°C for PEEK151 and 170°C for AM 200) and HAT in Region II (i.e. 200°C).

3.2.1 From SAXS

Figure 8 shows the raw SAXS spectra of as printed and annealed PEEK151 and AM 200 samples. For as printed samples, the absence of a diffraction peak confirmed current FFF print settings produced amorphous parts. Annealing is required to produce crystalline final

products. For annealed samples, the scattering intensity have maxima at q around 0.5 nm^{-1}, caused by the inter-lamella interference reflecting the long periodicity.

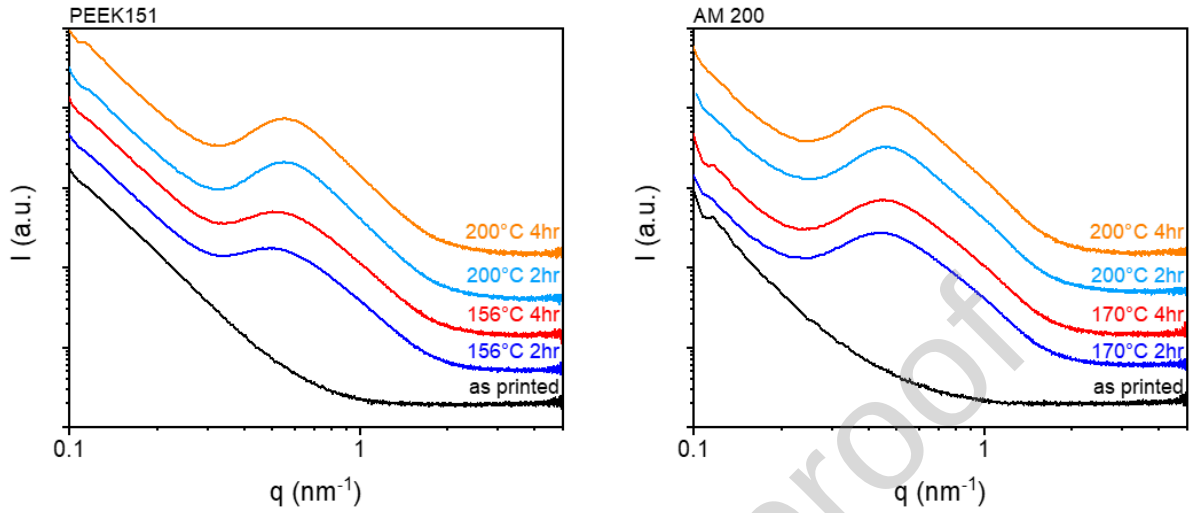

Figure 8. SAXS spectra for as printed and annealed samples. The curves were displayed vertically.

Lamellar dimensions can be accessed via a correlation function analysis [44]. In theory, the electron density distribution within the sample can be linked to the scattering intensity by

$$I(q) = \iint \rho(r_i)\rho(r_j)\, e^{-iq(r_i - r_j)} dV_{ri}\, V_{rj} \qquad \text{(Eq. 2)}$$

where q is the scattering vector, $I(q)$ is the measured intensity and $\rho(r_k)$ is the local electron density in volume element V_{rk} [45].

In an ideal two-phase lamellar model, the electron density can be considered as a periodic signal. Therefore, Fourier transform can be applied to extract the periodic characteristics, e.g. long period l_p and lamellar thickness l_c. The correlation function obtained by Fourier transform expressed as [46]:

$$\Gamma_1 = \frac{1}{Q}\int_0^\infty I(q) q^2 \cos(qr)\, dq \qquad \text{(Eq. 3)}$$

where Γ_1 is the one-dimensional correlation function, $I(q)$ is the measured intensity and Q is the scattering invariant given by $Q = \int_0^\infty I(q) q^2 dq$.

Prior to applying the Fourier transform, the raw spectra data was extrapolated to $q = 0$ by the Guinier function (Eq. 4) and to $q = \infty$ by a sigmoid function (Eq. 5) to fill the entire space [47][48].

$$I(q) = Ae^{Bq^2} \quad \text{(Eq. 4)}$$

where A and B are fitting parameters.

$$I(q) = B + Kq^{-4}e^{-q^2\sigma^2} \quad \text{(Eq. 5)}$$

where B is the thermal background, K is the Porod constant, and σ is related to the electron density.

After the extrapolation and transformation, l_p and l_c of annealed samples were deduced from the one-dimensional correlation function [48][49][50] as exampled in Figure 9. All lamellar dimensions and crystallinity are listed in Table 4.

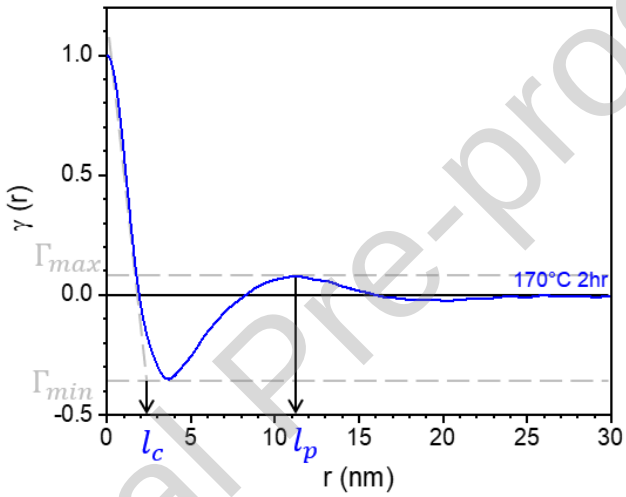

Figure 9. One-dimensional correlation function of AM 200 sample annealed at 170°C for 2 hr.

Table 4. Lamellar dimensions and crystallinity levels from SAXS.

Material	**Annealing conditions**	$l_p\ (nm)$	$l_c\ (nm)$	**Crystallinity (%)**
PEEK151	156 °C, 2 hr	9.20	2.14	23.3
	156 °C, 4 hr	9.02	2.12	23.5
	200 °C, 2 hr	9.00	2.20	24.5
	200 °C, 4 hr	9.09	2.18	23.9
AM 200	170 °C, 2 hr	11.30	2.34	20.8
	170 °C, 4 hr	10.50	2.37	22.6
	200 °C, 2 hr	11.10	2.43	21.9
	200 °C, 4 hr	11.10	2.46	22.2

It shows that crystal morphology remains more or less the same among the chosen annealing temperatures and annealing times. The potential causes are discussed in the following section.

3.2.2 From DSC

Another method to calculate the lamellar thickness is using the Thomson-Gibbs equation [51].

$$T_{\mathrm{m}} = T_{\mathrm{m}}^{0}\left(1 - \frac{2\sigma_{\mathrm{e}}}{\Delta H \times l_c \times \rho_c}\right) \quad \text{(Eq. 6)}$$

where T_{m} is the measured melting temperature, T_{m}^{0} is the equilibrium melting temperature of a crystal having infinite size, σ_{e} is the interfacial free energy, 49 erg/cm^3 for PAEKs, ΔH is the enthalpy of fusion per repeating unit, 130 J/g for PAEKs, l_c is the lamellar thickness, and ρ_{c} is crystalline density, 1.415 g/cm^3 [51].

The first step is to determine the equilibrium melting temperature by the Hoffman-Weeks method [52]. Melting temperature T_{m} measured from conventional DSC and flash DSC are plotted as a function of the isothermal crystallisation temperature T_{c} in Figure 10. Only upper endothermic temperatures were adopted for this method [38]. At the equilibrium temperature T_{m}^{0}, the lamellar thickness is considered to be infinite, resulting in the melting temperature equivalent to the crystallisation temperature. Therefore, a linear extrapolation towards the equilibrium condition ($T_{\mathrm{m}} = T_{\mathrm{c}}$) yields an intercept as the equilibrium melting temperature T_{m}^{0}.

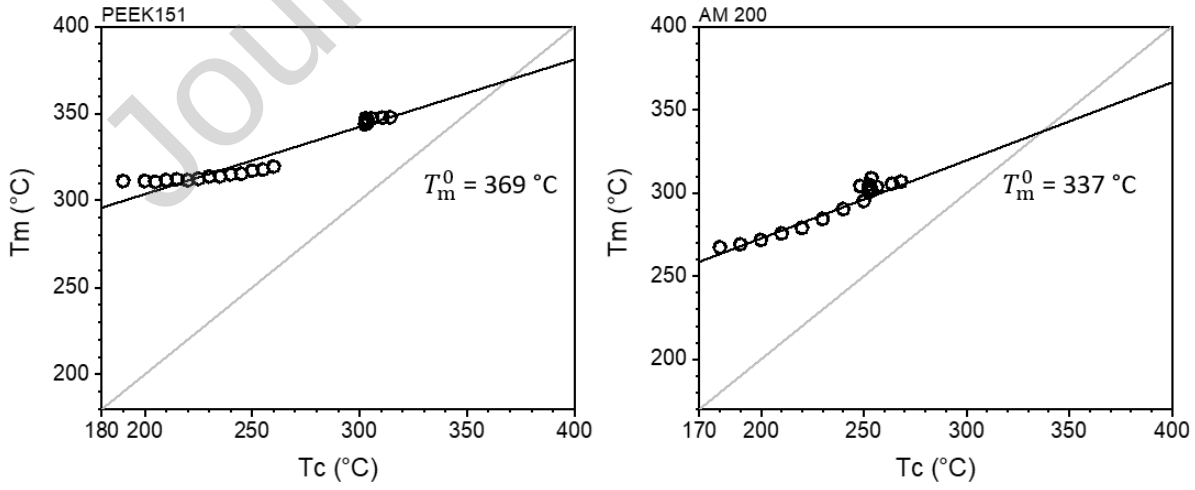

Figure 10. Melting temperature plotted as a function of crystallisation temperature.

The quantified T_{m}^{0} value of PEEK151 (369°C) is consistent with literature values ranging from 357 to 395°C [53][38][51]. In contrast, AM 200 exhibits a much lower T_{m}^{0}. The equilibrium

melting temperature was used further to calculate the lamella thicknesses of the two PAEK grades.

The isothermal tests revealed the presence of double melting peaks associated previously in the literature with two main theories. One suggests a melt – recrystallisation model where crystals of lower melting temperatures reorganize in thicker lamellae that melt at higher melting temperatures [51]. This theory is usually applied to explain the double endothermic peaks observed from conventional DSC. The second theory is based on a dual lamellar population model with two possible scenarios: 1) lamellar insertion where linear thinner lamellae form in between two thicker lamellae [50][54] and 2) dual lamellar stack where two-dimensional lamellae stack bundles form in molten liquid pockets between primary lamellar stacks [55]. The obtained crystallisation kinetics of the two PAEK grades seem to be in favour of the first scenario, as the secondary Avrami exponents are close to one, implying rather linear secondary lamellar structures.

To validate the dual lamellar population theory, flash DSC was used to measure the melting temperatures under a fast ramping rate that suppresses crystal reorganizing. For PEEK151 and AM 200, double melting peaks exist even under a heating rate of 1000 °C/s, representing two lamellar populations. Well-developed lamellae from primary crystallisation melt at high temperatures whilst less defined secondary lamellae formed by insertion melt at low temperatures [56][57]. For this reason, the double melting peaks were deconvoluted and considered separately in the calculation of the lamellae thickness. By substituting the peak temperatures back into Eq. 6, lamellar thicknesses of primary and secondary crystallisation were estimated as shown in Figure 11.

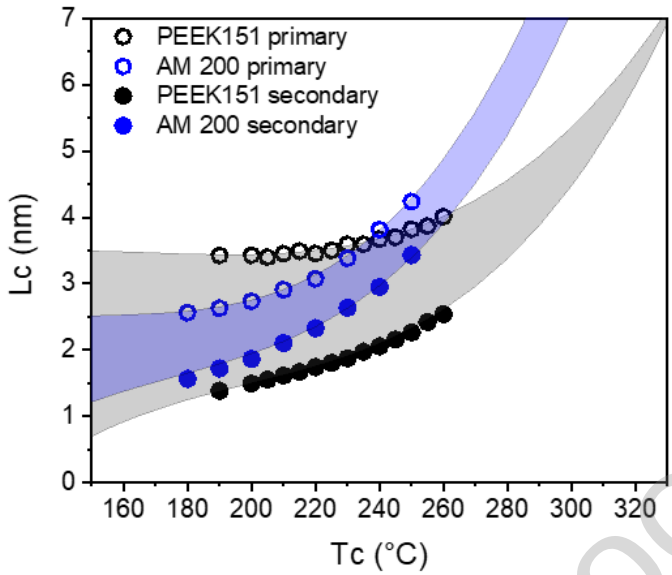

Figure 11. Calculated lamellar thickness plotted as a function of isothermal temperature. The boundaries of shaded areas are predictions based on experimental data.

The lamellar thicknesses show upward trends in relation to the increasing isothermal temperature T_c, resembling the trend reported by Cebe [33]. This trend could be originated from the fact that, forming lamellae is a molecular chain-folding process that needs to overcome a diffusion barrier. This barrier is very low near the melting point, thus easy to form thicker lamellae, and very high near the glass transition temperature, leading to thinner lamellae [58].

In general, AM 200 displays stronger temperature dependence indicated by steeper slopes. The upward trends of AM 200's primary and secondary lamellar thicknesses seem to be parallel while those of PEEK151 converge towards higher isothermal temperature. In addition, the shaded areas illustrate that, at the low temperature region (< 200°C) lamellar thickness is less sensitive to temperature than at the high temperature region (> 200°C).

It is noted that, when treating the annealing temperature as T_c, lamellar thickness from SAXS (in Table 4) can be found in between the primary and secondary lamellar thicknesses. The values are reasonable considering the SAXS lamellar thicknesses are azimuthally averaged values. The insignificant effects of annealing temperature and annealing time on lamellar thickness are in line with the insensitivity to temperature at the low temperature region. One possible reason is that, due to the bulky molecular chains, the friction barrier could be too high to initiate thickening via chain-sliding diffusion at this temperature region

once crystals are formed [58]. Nevertheless, for practical reasons, the annealing temperatures (156°C for PEEK151 and 170°C for AM 200) were selected based on slow crystallisation half-times to avoid warpage induced by fast crystallisation. In FFF processing, the benefits of thick lamellae against structural distortion at high temperature region should be weighed with caution.

3.3 Mechanical properties

The low build temperature of the printer allowed the printing amorphous parts of both PAEK grades, which upon annealing enhanced the mechanical properties. Standard tensile tests were performed to examine the mechanical properties of both polymers by comparison as printed and annealed. Elastic modulus, tensile strength, and elongation at break of each build orientation and each annealing condition were summarised in Figure 12. Typical stress-strain curves for each condition (closest to the mean values) are displayed in Figure 13.

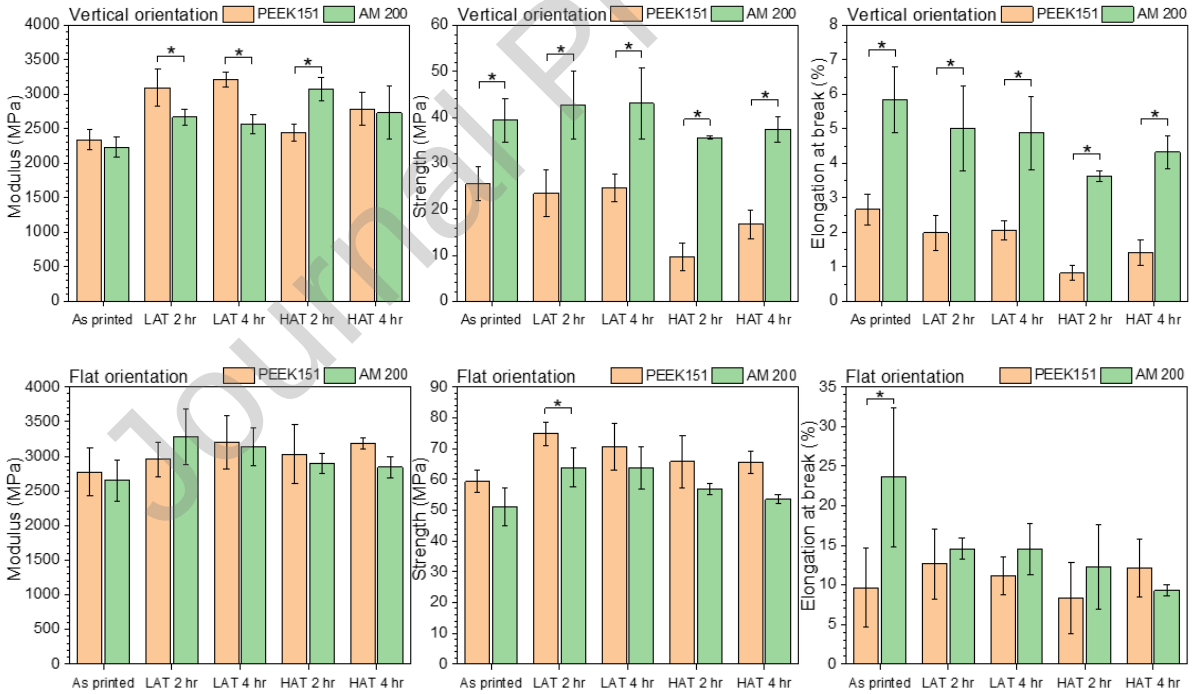

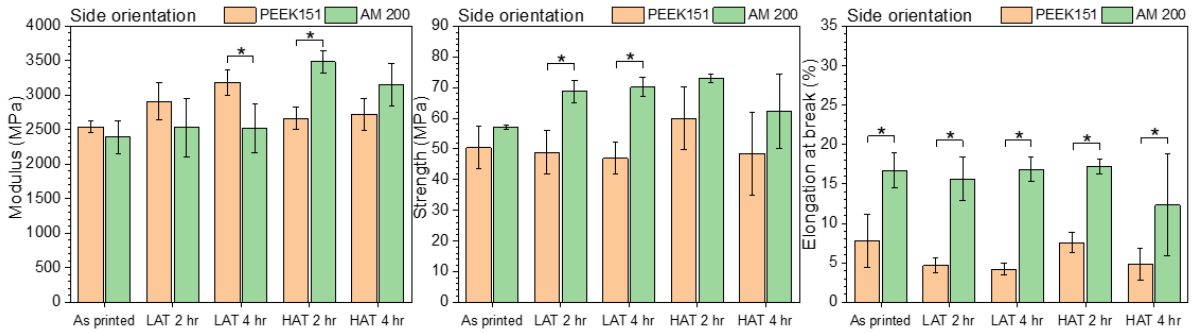

Figure 12. Mechanical properties of as printed and annealed samples. Any significant difference within a pair is marked by an asterisk bracket.

The benefit of using a slow crystallising grade such as AM 200 in FFF is evidenced by the mechanical results in vertical orientation. Statistical analyses show that there are significant differences in Z modulus, Z strength and Z elongation at break values between AM 200 and PEEK151, independent of the annealing temperature or the annealing time. AM 200 specimens have Z strength values around 40 MPa, which is markedly higher than the Z strength of PEEK151 specimens which are around 25 MPa. They are also substantially higher than the Z strength values reported by Arif et al [11] (9.99 MPa for PEEK450) and Rinaldi et al [12] (19.6 MPa for PEEK450).

In general, PEEK151 exhibits strong orientation dependency; its Z strength is around 30% of flat and side strength. By sharp contrast, the Z strength of AM 200 is approximately 60% of flat and side strength, hence more isotropic. These differences could be attributed to the different crystallisation kinetics in addition to build orientation effects. For flat and side tensile bars, the loading direction is 45° to the raster fill direction, whilst for Z bars the loading direction is perpendicular to the layer surface. The different stress transmission patterns result in the build orientation dependency. Moreover, slow crystallisation featured by large half-times and high Avrami exponents promotes well developed spherulitic structures, which many authors have concluded is the key to better mechanical properties [33][25][27]. Additionally, the secondary crystal evolution might be more significant in an FFF process than in a conventional moulded process, since layer to layer bonding is dominating. Jar et al [34] speculated the enhancement comes from reorganisation of inter-lamellar structures from secondary crystallisation, which has been confirmed later by Hsiao et al [54] and Wang et al [50] using time-resolved SAXS. In this study, the dual-Avrami exponents of two PAEK polymers support that linear lamellae inserts between primary

lamellae. At the selected annealing temperatures, PEEK151 has similar K_1 and K_2 whilst AM 200 has higher K_2 than K_1. It suggests that the intrinsic property of AM 200 promotes secondary crystallisation. Combining with the slow crystallising nature, AM 200 displays stronger layer adhesion contributing to higher Z strength.

Although the authors have no experimental evidence for it happening in FFF process yet, a study on UHMWPE by Xue et al [59] shows, for semi-crystalline polymers, that crystallisation can take place across the interface of two layers at temperatures above T_g when intimate contact is achieved. According to Xue et al, the cross-layer-crystallisation can be prohibited by 'pre-annealing' one side of the interface. Applying the same theory here, it is possible that for a fast crystallising grades such as PEEK151, quickly formed crystals on the surface are blocking crystallisation across the layers, leading to weak interlayer bonding, and ultimately weak Z properties. This theory could explain the lower Z strength of PEEK 151 in comparison with AM200.

For flat and side specimens, the majority of elongation at break values were obtained beyond the yield point, representing the true ductility. On the other hand, all Z specimens failed prematurely before yielding, as demonstrated in Figure 13. The Z elongation at break values are positively proportional to the tensile strength, reflecting the interlayer bonding rather than ductility. The elongation at break values of AM 200 are higher than that of PEEK151, possibly due to the crystal structures of PEEK151 being less perfect as implied by the low Avrami exponents and the fast crystallising speed. This morphology might produce more crystal defects weakening the layer to layer bonding, eventually leading to brittle failure.

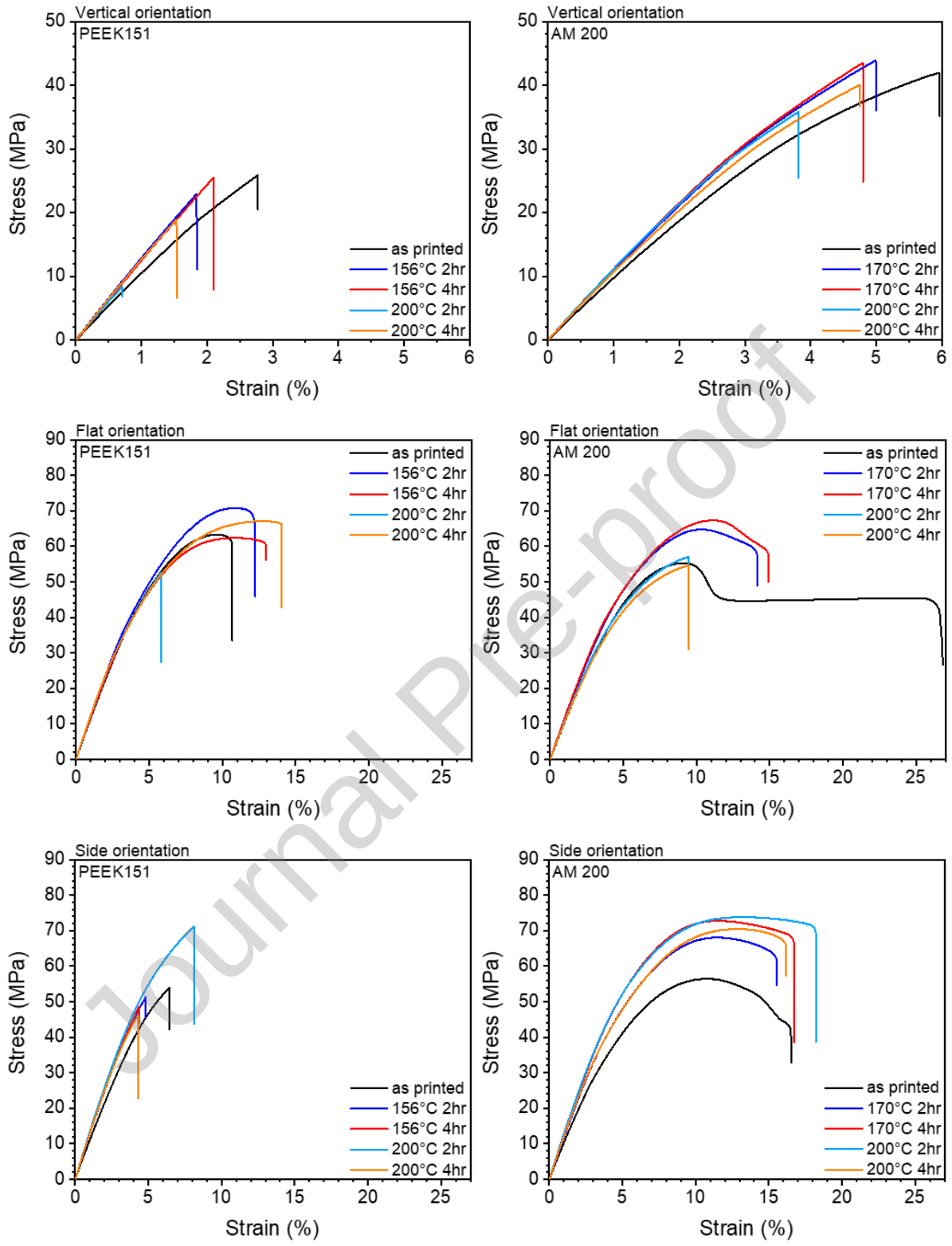

Figure 13. Typical stress-strain curves of vertical, flat, and side specimens.

Annealed AM 200 specimens have a lower elongation at break than the as printed amorphous specimens. It could be argued that “as printed” specimens could be used for components and parts without any other post-treatment. However, this would lead to

significant distortion of the part under high service temperature, due to a) the complexity of the printed part and its deposition strategy combined with b) the shrinkage effects unavoidably created by the spontaneous crystallisation of parts when used in thermal environments or in mechanically demanding applications where heat is generated. Therefore, controlled annealing in a slow crystallisation rate fashion is required to minimize the risk of warping caused by rapid heating.

Amorphous PEEK151 and AM 200 have similar moduli around 2500 MPa. Annealing generally improves the moduli. A higher annealing temperature seems to work better for AM 200 than for PEEK151. This could be due to the stronger temperature dependence highlighted in Figure 11. The improvement in moduli observed in this study, especially for Z samples, might be due to better layer adhesion induced by annealing. The effect of increasing annealing time is not evident, which is consistent with the work of Jar et al [34].

4. Conclusions

In this study, crystallisation kinetics of the commercialised grade PEEK151 and the novel grade AM 200 were captured in a wide temperature range. AM 200 was identified as a slow crystallising PAEK revealed by the crystallisation half-times. A dual-Avrami model has been successfully implemented on both grades. Avrami exponents and rate constants suggest that AM 200 forms better defined primary crystals complemented with a relatively high rate of secondary lamellae insertion, contributing to higher isotropy in printed parts than PEEK151.

The morphology of two lamellar populations were examined by flash DSC. By deconvoluting the double endothermic peaks, a relationship between primary and secondary lamellar thicknesses and isothermal crystallisation temperatures was discovered. The diffusion and friction barrier theories help explain why increasing annealing temperature or annealing time at a low temperature range has no significant effect on lamellar thickness or crystallinity.

Upon annealing, both polymeric grades showed overall some improvement in the mechanical performance less the elongation at break – a phenomenon well established amongst semi-crystalline polymers exposed to annealing treatments. A method to select annealing temperatures and annealing times based on crystallisation half-times was

proposed. The benefits of adopting slow crystallising PAEKs with a high rate of secondary crystallisation for the FFF process were demonstrated, including higher Z strength, higher tensile strengths, and elongation. These findings highlight the importance of designing dedicated polymers for the FFF process, with a focus on their intrinsic crystallisation behaviour which ultimately leads to improved isotropy.

Declaration of competing interest

The authors declare no conflict of interest.

Acknowledgements

The authors thank Dr Rémi Castaing of the Material and Chemical Characterisation Facility (MC²) at University of Bath (https://doi.org/10.15125/mx6j-3r54) for his technical support and assistance in SAXS experiments.

Appendix

Supplementary materials associated with this article can be found.

References

[1] D. P. Jones, D. C. Leach, and D. R. Moore, "Mechanical properties of poly(ether-ether-ketone) for engineering applications," *Polymer (Guildf).*, vol. 26, no. 9, pp. 1385–1393, 1985, doi: 10.1016/0032-3861(85)90316-7.

[2] R. I. Shekar, T. M. Kotresh, P. M. D. Rao, and K. Kumar, "Properties of high modulus PEEK yarns for aerospace applications," *J. Appl. Polym. Sci.*, vol. 112, no. 4, pp. 2497–2510, May 2009, doi: 10.1002/app.29765.

[3] K. H. Tan *et al.*, "Scaffold development using selective laser sintering of polyetheretherketone-hydroxyapatite biocomposite blends," *Biomaterials*, vol. 24, no. 18, pp. 3115–3123, 2003, doi: 10.1016/S0142-9612(03)00131-5.

[4] S. Berretta, K. E. Evans, and O. Ghita, "Processability of PEEK, a new polymer for high temperature laser sintering (HT-LS)," *Eur. Polym. J.*, vol. 68, pp. 243–266, 2015, doi: 10.1016/j.eurpolymj.2015.04.003.

[5] B. Valentan, Ž. Kadivnik, T. Brajlih, A. Anderson, and I. Drstvenšek, "Processing poly(ether etherketone) on a 3d printer for thermoplastic modelling," *Mater. Tehnol.*, vol. 47, no. 6, pp. 715–721, 2013.

[6] J. F. Rodriguez, J. P. Thomas, and J. E. Renaud, "Characterization of the mesostructure of fused-deposition acrylonitrile-butadiene-styrene materials," *Rapid Prototyp. J.*, vol. 6, no. 3, pp. 175–185, 2000, doi: 10.1108/13552540010337056.

[7] M. H. Too *et al.*, "Investigation of 3D non-random porous structures by fused

deposition modelling," *Int. J. Adv. Manuf. Technol.*, vol. 19, no. 3, pp. 217–223, 2002, doi: 10.1007/s001700200016.

[8] K. C. Ang, K. F. Leong, C. K. Chua, and M. Chandrasekaran, "Investigation of the mechanical properties and porosity relationships in fused deposition modelling-fabricated porous structures," *Rapid Prototyp. J.*, vol. 12, no. 2, pp. 100–105, 2006, doi: 10.1108/13552540610652447.

[9] Y. Liao *et al.*, "Effect of porosity and crystallinity on 3D printed PLA properties," *Polymers (Basel).*, vol. 11, no. 9, pp. 1–14, 2019, doi: 10.3390/polym11091487.

[10] Victrex PLC, "Victrex and Bond pioneer 3D printing for PAEK parts with maximized performance" *https://www.victrex.com/en/news/2019/03/victrex-bond-3d-parts*, viewed 24 June 2020.

[11] M. F. Arif, S. Kumar, K. M. Varadarajan, and W. J. Cantwell, "Performance of biocompatible PEEK processed by fused deposition additive manufacturing," *Mater. Des.*, vol. 146, pp. 249–259, 2018, doi: 10.1016/j.matdes.2018.03.015.

[12] M. Rinaldi, T. Ghidini, F. Cecchini, A. Brandao, and F. Nanni, "Additive layer manufacturing of poly (ether ether ketone) via FDM," *Compos. Part B Eng.*, vol. 145, no. December 2017, pp. 162–172, 2018, doi: 10.1016/j.compositesb.2018.03.029.

[13] C. Yang, X. Tian, D. Li, Y. Cao, F. Zhao, and C. Shi, "Influence of thermal processing conditions in 3D printing on the crystallinity and mechanical properties of PEEK material," *J. Mater. Process. Technol.*, vol. 248, no. January, pp. 1–7, 2017, doi: 10.1016/j.jmatprotec.2017.04.027.

[14] Stepashkin, D. I. Chukov, F. S. Senatov, A. I. Salimon, A. M. Korsunsky, and S. D. Kaloshkin, "3D-printed PEEK-carbon fiber (CF) composites: Structure and thermal properties," *Compos. Sci. Technol.*, vol. 164, no. January, pp. 319–326, 2018, doi: 10.1016/j.compscitech.2018.05.032.

[15] M. Vaezi and S. Yang, "Extrusion-based additive manufacturing of PEEK for biomedical applications," *Virtual Phys. Prototyp.*, vol. 10, no. 3, pp. 123–135, 2015, doi: 10.1080/17452759.2015.1097053.

[16] G. M. K. Ostberg and J. C. Seferis, "Annealing effects on the crystallinity of polyetheretherketone (PEEK) and its carbon fiber composite," *J. Appl. Polym. Sci.*, vol. 33, no. 1, pp. 29–39, 1987, doi: 10.1002/app.1987.070330103.

[17] H. Gupta and R. Salovey, "Thermal behavior of transparent poly(etheretherketone)(PEEK) film," *Polym. Eng. Sci.*, vol. 30, no. 8, pp. 453–458, 1990, doi: 10.1002/pen.760300805.

[18] J. J. C. Cruz-Pinto, J. A. Martins, and M. J. Oliveira, "The isothermal crystallization of engineering polymers - POM and PEEK," *Colloid Polym. Sci.*, vol. 272, no. 1, pp. 1–16, 1994, doi: 10.1007/BF00653305.

[19] F. J. Medellín-Rodríguez and P. J. Phillips, "Bulk crystallization of poly(aryl ether ether ketone) (PEEK)," *Polym. Eng. Sci.*, vol. 36, no. 5, pp. 703–712, 1996, doi: 10.1002/pen.10457.

[20] A. Lustiger, F. S. Uralil, and G. M. Newaz, “Processing and structural optimization of PEEK composites,” *Polym. Compos.*, vol. 11, no. 1, pp. 65–75, 1990, doi: 10.1002/pc.750110109.

[21] S. Berretta, K. E. Evans, and O. R. Ghita, “Predicting processing parameters in high temperature laser sintering (HT-LS) from powder properties,” *Mater. Des.*, vol. 105, pp. 301–314, 2016, doi: 10.1016/j.matdes.2016.04.097.

[22] R. A. Chivers and D. R. Moore, “The effect of molecular weight and crystallinity on the mechanical properties of injection moulded poly(aryl-ether-ether-ketone) resin,” *Polymer (Guildf).*, vol. 35, no. 1, pp. 110–116, 1994, doi: 10.1016/0032-3861(94)90057-4.

[23] E. W. Fischer, “Effect Of Annealing And Temperature On The Morphological Structure Of Polymers,” *Pure Appl. Chem.*, vol. 31, no. 1–2, pp. 113–132, 1972, doi: 10.1351/pac197231010113.

[24] J. Petermann, M. Miles, and H. Gleiter, “Growth of Polymer Crystals during Annealing,” *J. Macromol. Sci. Part B*, vol. 12, no. 3, pp. 393–404, 1976, doi: 10.1080/00222347608019327.

[25] A. Arzak, J. I. Eguiazábal, and J. Nazábal, “Effect of annealing on the properties of poly(ether ether ketone),” *Polym. Eng. Sci.*, vol. 31, no. 8, pp. 586–591, 1991, doi: 10.1002/pen.760310809.

[26] V. Mylläri, T. P. Ruoko, J. Vuorinen, and H. Lemmetyinen, “Characterization of thermally aged polyetheretherketone fibres - Mechanical, thermal, rheological and chemical property changes,” *Polym. Degrad. Stab.*, vol. 120, pp. 419–426, 2015, doi: 10.1016/j.polymdegradstab.2015.08.003.

[27] Z. Jiang, M. Mullins, H. J. Sue, and T. Bremner, “Effect of annealing on the viscoelastic behavior of poly(ether-ether-ketone),” *Annu. Tech. Conf. - ANTEC, Conf. Proc.*, vol. 2018-May, no. November 2018, pp. 231–237, 2018.

[28] A. Bagsik, V. Schöppner, and E. Klemp, “FDM Part Quality Manufactured with Ultem*9085,” *Int. Conf. Polym. Mater. 2010 Halle, Saale*, vol. 1, 2010.

[29] M. Fischer and V. Schöppner, “Fatigue Behavior of FDM Parts Manufactured with Ultem 9085,” *Jom*, vol. 69, no. 3, pp. 563–568, 2017, doi: 10.1007/s11837-016-2197-2.

[30] 3DXTECH, *https://www.3dxtech.com/ultra-performance-filaments/thermax-pekk-c/*, viewed 24 June 2020.

[31] F. Awaja and S. Zhang, “Self-bonding of PEEK for active medical implants applications,” *J. Adhes. Sci. Technol.*, vol. 29, no. 15, pp. 1593–1606, 2015, doi: 10.1080/01694243.2015.1037382.

[32] M. F. Talbott, G. S. Springer, and L. A. Berglund, “The Effects of Crystallinity on the Mechanical Properties of PEEK Polymer and Graphite Fiber Reinforced PEEK,” *J. Compos. Mater.*, vol. 21, no. 11, pp. 1056–1081, 1987, doi: 10.1177/002199838702101104.

[33] P. Cebe, “Annealing study of poly(etheretherketone),” *J. Mater. Sci.*, vol. 23, no. 10,

pp. 3721–3731, Oct. 1988, doi: 10.1007/BF00540520.

[34] P. Y. Jar, H. H. Kausch, W. J. Cantwell, P. Davies, and H. Richard, "The effect of annealing on the short and long term behavior of PEEK," *Polym. Bull.*, vol. 24, no. 6, pp. 657–664, Dec. 1990, doi: 10.1007/BF00300163.

[35] C. Basgul, T. Yu, D. W. MacDonald, R. Siskey, M. Marcolongo, and S. M. Kurtz, "Does annealing improve the interlayer adhesion and structural integrity of FFF 3D printed PEEK lumbar spinal cages?," *J. Mech. Behav. Biomed. Mater.*, vol. 102, no. September 2019, p. 103455, Feb. 2020, doi: 10.1016/j.jmbbm.2019.103455.

[36] M. Day, Y. Deslandes, J. Roovers, and T. Suprunchuk, "Effect of molecular weight on the crystallization behaviour of poly(aryl ether ether ketone): a differential scanning calorimetry study," *Polymer (Guildf).*, vol. 32, no. 7, pp. 1258–1266, 1991, doi: 10.1016/0032-3861(91)90230-G.

[37] X. Tardif *et al.*, "Experimental study of crystallization of PolyEtherEtherKetone (PEEK) over a large temperature range using a nano-calorimeter," *Polym. Test.*, vol. 36, pp. 10–19, 2014, doi: 10.1016/j.polymertesting.2014.03.013.

[38] J. Seo *et al.*, "Isothermal crystallization of poly(ether ether ketone) with different molecular weights over a wide temperature range," *Polym. Cryst.*, vol. 2, no. 1, 2019, doi: 10.1002/pcr2.10055.

[39] P. Cebe and S. D. Hong, "Crystallization behaviour of poly(ether-ether-ketone)," *Polymer (Guildf).*, vol. 27, no. 8, pp. 1183–1192, 1986, doi: 10.1016/0032-3861(86)90006-6.

[40] C. N. Velisaris and J. C. Seferis, "Crystallization kinetics of polyetheretherketone (peek) matrices," *Polym. Eng. Sci.*, vol. 26, no. 22, pp. 1574–1581, 1986, doi: 10.1002/pen.760262208.

[41] I. H. Hillier, "Modified avrami equation for the bulk crystallization kinetics of spherulitic polymers," *J. Polym. Sci. Part A Gen. Pap.*, vol. 3, no. 9, pp. 3067–3078, 1965, doi: 10.1002/pol.1965.100030902.

[42] T. Choupin, B. Fayolle, G. Régnier, C. Paris, J. Cinquin, and B. Brulé, "Isothermal crystallization kinetic modeling of poly(etherketoneketone) (PEKK) copolymer," *Polymer (Guildf).*, vol. 111, pp. 73–82, 2017, doi: 10.1016/j.polymer.2017.01.033.

[43] T. Liu, Z. Mo, S. Wang, and H. Zhang, "Isothermal melt and cold crystallization kinetics of poly(aryl ether ether ketone ketone) (PEEKK)," *Eur. Polym. J.*, vol. 33, no. 9, pp. 1405–1414, 1997, doi: 10.1016/S0014-3057(97)00016-5.

[44] G. R. Strobl and M. Schneider, "Direct Evaluation of the Electron Density Correlation Function of Partially Crystalline Polymers.," *J. Polym. Sci. Part A-2, Polym. Phys.*, vol. 18, no. 6, pp. 1343–1359, 1980.

[45] P. Debye, H. R. Anderson, and H. Brumberger, "Scattering by an inhomogeneous solid. II. the correlation function and its application," *J. Appl. Phys.*, vol. 28, no. 6, pp. 679–683, 1957, doi: 10.1063/1.1722830.

[46] W. Wang, J. M. Schultz, and B. S. Hsiao, "Time-Resolved Simultaneous SAXS/WAXS

Studies of PEEK during Isothermal Crystallization, Melting, and Subsequent Cooling," *J. Macromol. Sci. - Phys.*, vol. 37, no. 5, pp. 667–682, 1998, doi: 10.1080/00222349808212408.

[47] J. T. Koberstein, B. Morra, and R. S. Stein, "The determination of diffuse-boundary thicknesses of polymers by small-angle X-ray scattering," *J. Appl. Crystallogr.*, vol. 13, no. 1, pp. 34–45, Feb. 1980, doi: 10.1107/S0021889880011478.

[48] F. J. Medellín-Rodríguez, P. J. Phillips, and J. S. Lin, "Application of Secondary Nucleation Theory to Semirigid Macromolecules: PEEK, PET, and PEN," *Macromolecules*, vol. 28, no. 23, pp. 7744–7755, 1995, doi: 10.1021/ma00127a022.

[49] A. M. Jonas, D. A. Ivanov, and D. Y. Yoon, "The semicrystalline morphology of poly(ether-ether-ketone) blends with poly(ether-imide)," *Macromolecules*, vol. 31, no. 16, pp. 5352–5362, 1998, doi: 10.1021/ma9711607.

[50] J. Wang *et al.*, "Synchrotron Small-angle X-ray Scattering Study of Crystalline Structures and Isothermal Crystallization Kinetics of Poly(aryl ether ether ketones)," *Macromolecules*, vol. 25, no. 25, pp. 6943–6951, 1992, doi: 10.1021/ma00051a035.

[51] Y. Lee, R. S. Porter, and J. S. Lin, "On the Double-Melting Behavior of Poly(ether ether ketone)," *Macromolecules*, vol. 22, no. 4, pp. 1756–1760, 1989, doi: 10.1021/ma00194a043.

[52] J. D. Hoffman and J. J. Weeks, "Melting process and the equilibrium melting temperature of polychlorotrifluoroethylene," *J. Res. Natl. Bur. Stand. Sect. A Phys. Chem.*, vol. 66A, no. 1, p. 13, 1962, doi: 10.6028/jres.066a.003.

[53] B. de Carvalho and R. E. S. Bretas, "Crystallization kinetics of a PEEK/LCP blend," *J. Appl. Polym. Sci.*, vol. 55, no. 2, pp. 233–246, 1995, doi: 10.1002/app.1995.070550206.

[54] B. S. Hsiao, K. C. H. Gardner, D. Q. Wu, and B. Chu, "Time-resolved X-ray study of poly(aryl ether ether ketone) crystallization and melting behaviour: 1. Crystallization," *Polymer (Guildf).*, vol. 34, no. 19, pp. 3986–3995, 1993, doi: 10.1016/0032-3861(93)90658-W.

[55] R. K. Verma, V. Velikov, R. G. Kander, H. Marand, B. Chu, and B. S. Hsiao, "SAXS studies of lamellar level morphological changes during crystallization and melting in PEEK," *Polymer (Guildf).*, vol. 37, no. 24, pp. 5357–5365, 1996, doi: 10.1016/S0032-3861(96)00387-4.

[56] D. C. Bassett, R. H. Olley, and I. A. M. Al Raheil, "On crystallization phenomena in PEEK," *Polymer (Guildf).*, vol. 29, no. 10, pp. 1745–1754, 1988, doi: 10.1016/0032-3861(88)90386-2.

[57] S. Z. D. Cheng, M. Y. Cao, and B. Wunderlich, "Glass Transition and Melting Behavior of Poly(oxy-1,4-phenyleneoxy-1,4-phenylenecarbonyl-1,4-phenylene)," *Macromolecules*, vol. 19, no. 7, pp. 1868–1876, 1986, doi: 10.1021/ma00161a015.

[58] W. Hu, "The physics of polymer chain-folding," *Phys. Rep.*, vol. 747, pp. 1–50, 2018, doi: 10.1016/j.physrep.2018.04.004.

[59] Y. Q. Xue, T. A. Tervoort, S. Rastogi, and P. J. Lemstra, "Welding behavior of

semicrystalline polymers. 2. Effect of cocrystallization on autoadhesion," *Macromolecules*, vol. 33, no. 19, pp. 7084–7087, 2000, doi: 10.1021/ma000754y.

Highlights

- Slow crystallising AM 200 shows improvement in Z strength
- Lamellar thickness of AM 200 displays stronger temperature dependence
- Annealing provides modest improvement on the mechanical properties
- Annealing temperatures and times can be selected based on crystallisation behaviours
- This study provides insight into designing dedicated polymers for FFF process

Graphical abstract

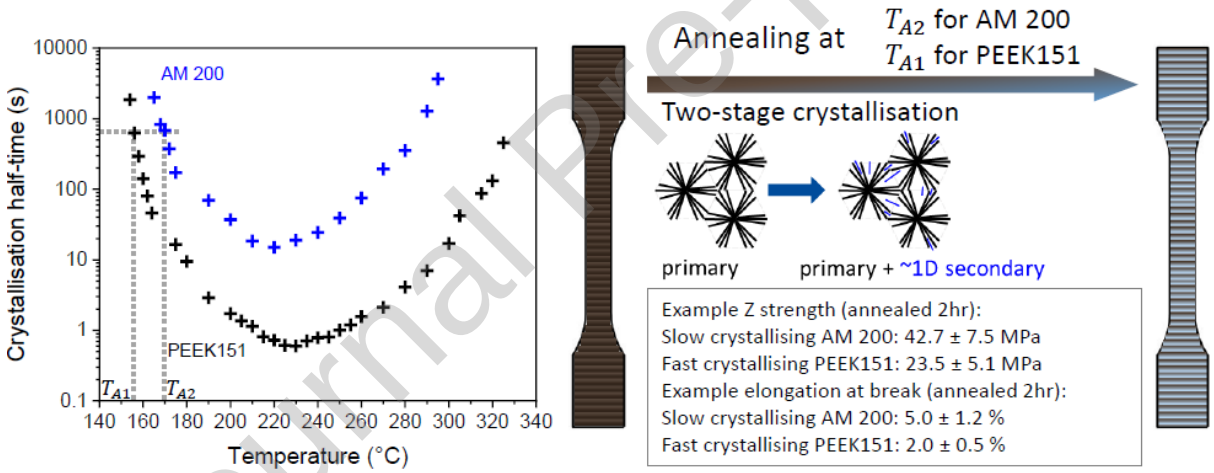

Author contributions

Nan Yi: Investigation, Formal analysis, Writing - Original Draft

Richard Davies: Methodology, Writing- Reviewing & Editing

Adam Champlin: Resources, Writing- Reviewing & Editing

Paul McCutchion: Project administration, Writing - Review & Editing

Oana Ghita: Conceptualization, Supervision, Writing - Review & Editing

Declaration of interests

☒ The authors declare that they have no known competing financial interests or personal relationships that could have appeared to influence the work reported in this paper.

☐The authors declare the following financial interests/personal relationships which may be considered as potential competing interests: